The EMBO Journal vol.14 no.22 pp.5514–5523, 1995

Influenza hemagglutinin assumes a tilted conformation during membrane fusion as determined by attenuated total reflection FTIR spectroscopy

Suren A.Tatulian, Peter Hinterdorfer[1], Gwen Baber and Lukas K.Tamm[2]

Department of Molecular Physiology and Biological Physics, University of Virginia School of Medicine, Charlottesville, VA 22908, USA
[1]Present address: Institute of Biophysics, University of Linz, 4040 Linz, Austria

[2]Corresponding author

Fusion of influenza virus with target membranes is mediated by an acid-induced conformational change of the viral fusion protein hemagglutinin (HA) involving an extensive reorganization of the α-helices. A 'spring-loaded' displacement over at least 100 Å provides a mechanism for the insertion of the fusion peptide into the target membrane, but does not explain how the two membranes are brought into fusion contact. Here we examine, by attenuated total reflection Fourier transform infrared spectroscopy, the secondary structure and orientation of HA reconstituted in planar membranes. At neutral pH, the orientation of the HA trimers in planar membranes is approximately perpendicular to the membrane. However, at the pH of fusion, the HA trimers are tilted 55–70° from the membrane normal in the presence or absence of bound target membranes. In the absence of target membranes, the overall secondary structure of HA at the fusion pH is similar to that at neutral pH, but ~50–60 additional residues become α-helical upon the conformational change in the presence of bound target membranes. These results are discussed in terms of a structural model for the fusion intermediate of influenza HA.

Keywords: conformational change/Fourier transform infrared spectroscopy/influenza virus hemagglutinin/membrane fusion/supported membrane

Introduction

Hemagglutinin (HA) is the major glycoprotein of the influenza virus envelope. It is responsible for the binding of influenza virus to sialic acid-containing receptors on the surface of target cells and, after endocytosis, for the fusion of the viral and endosomal membranes (for recent reviews, see White, 1992; Clague *et al.*, 1993; Stegmann and Helenius, 1993). Influenza HA is a homotrimer with a total M_r of ~230 kDa. Each subunit consists of two disulfide-linked polypeptide chains, HA1 and HA2. HA1 forms the larger part of the ectodomain of the protein and includes the receptor binding site. HA2 is anchored in the viral membrane by a single transmembrane peptide near its C-terminus. The N-terminus of HA2, which is known as the 'fusion peptide', is a highly conserved sequence of ~20 mostly apolar residues.

Each HA trimer projects as an elongated 'spike' ~135 Å from the viral membrane surface. The crystal structure of the ectodomain of HA (called BHA) at neutral pH is known to 3 Å resolution (Wilson *et al.*, 1981). The backbone of the homotrimer is formed by a coiled-coil of three ~80 Å long α-helices. Three globular domains sit on top of a narrower stem region. The fusion peptide is buried in the stem region in the pH 7 crystal structure. In the intact HA molecule it is expected to reside ~35 Å above the surface of the viral membrane and ~100 Å from the receptor binding site at the top of the molecule. Membrane fusion is triggered by the low pH that prevails in the endosome. A large conformational change (Skehel *et al.*, 1982; Doms *et al.*, 1985), during which the fusion peptide becomes inserted into the target membrane (Harter *et al.*, 1989; Stegmann *et al.*, 1991; Tsurudome *et al.*, 1992), occurs below a critical pH of ~5.0–6.0 and leads ultimately to the fusion of viral and target membranes. These observations immediately raised two important questions about the structure of HA at the site of membrane fusion: (i) how is it possible to insert the fusion peptide into the target membrane that is at least 100 Å away from its location in the bound state at neutral pH?; and (ii) how are the viral and target membranes, which at neutral pH are separated by the 135 Å long trimers, brought to close fusion contact? Two recent studies provided new insight and at least a partial answer to the first question. Based on molecular modeling and circular dichroism (CD) experiments on peptides corresponding to the helical stem and the N-terminally adjacent loop region, Carr and Kim (1993) proposed a 'spring-loaded' mechanism for the conformational change of influenza HA, in which the fusion peptide is propelled close to the top of the molecule (where it now could reach the target membrane) by an N-terminal extension of the triple-stranded coiled-coil. The crystal structure of a fragment (called TBHA2) of the ectodomain at low pH, which comprises most of the HA2 subunit (but lacks the 39 most N-terminal residues, including the fusion peptide; Bullough *et al.*, 1994), confirmed and extended Carr and Kim's proposal. This fragment comprises a 100 Å long triple-stranded α-helical coiled-coil at its N-terminus. In addition, part of the original helical coiled-coil at pH 7 is broken near its C-terminus and reverses its direction. Although these studies explain the relocation of the fusion peptide towards the target membrane, they still do not provide a mechanism for the fusion process. In order to understand the mechanism of HA-mediated membrane fusion it is crucial to know how the HA molecules are oriented relative to the viral and target membranes at the pH of fusion and how the conformational change of HA brings the two membranes into fusion contact.

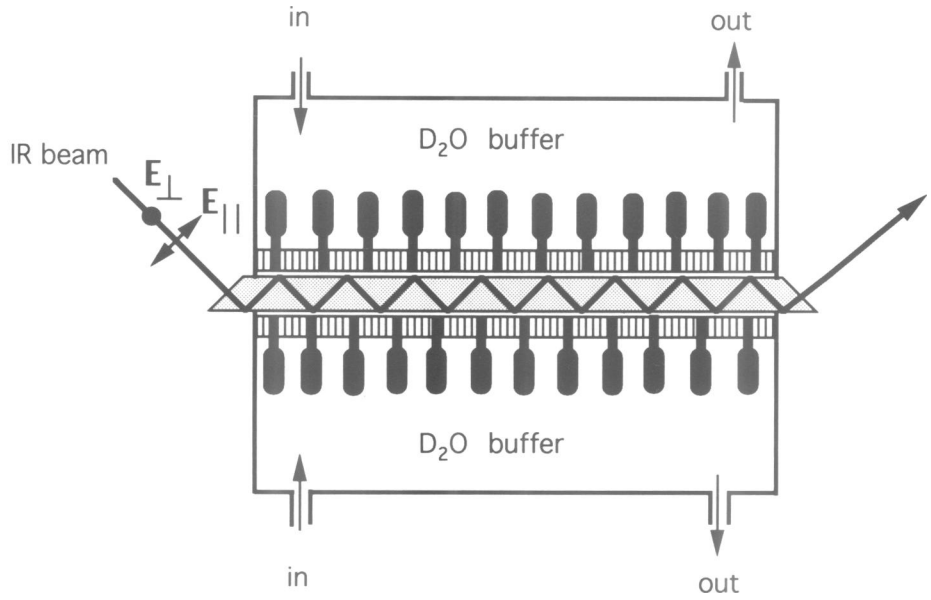

Fig. 1. Schematic depiction of the liquid ATR-FTIR measuring cell with hemagglutinin reconstituted in two supported planar lipid bilayers. The shaded flat trapezoid is the germanium internal reflection plate. The two dashed layers on each side of the plate represent the supported lipid bilayers with reconstituted HA (filled grenade-shaped symbols). In this system, >90% of all HA molecules are oriented with their ectodomain facing the large aqueous compartments of the measuring cell (Hinterdorfer *et al.*, 1994). The IR beam undergoes several internal reflections (of which ~36 are in the area covered with the supported membranes), exits the plate and is directed to the detector. $\mathbf{E}_\perp$ and $\mathbf{E}_{||}$ are the electric vectors of the IR beam polarized perpendicular and parallel to the plane of incidence, respectively. The two halves of the cell are interconnected (not shown) and can be flushed simultaneously with solutions or vesicle dispersions.

Here we have taken a new approach to address the question of the orientation of HA under various conditions. Recently, we have reconstituted purified HA into supported planar bilayers and we have shown that HA is functional in this system, because: (i) it can undergo pH-induced conformational change; (ii) it specifically binds target lipid bilayers at neutral pH; and (iii) it induces fusion of bound target vesicles when the pH is decreased to 5 (Hinterdorfer *et al.*, 1994). In this work, we use this oriented membrane system to characterize, by attenuated total reflection (ATR) Fourier transform infrared (FTIR) spectroscopy, the structural changes that occur when the pH is changed from 7.4 to 5 in the presence or absence of bound target membranes. We report the first direct observation of a prominent tilt of the HA molecules toward the plane of the membrane at low pH, which may be a critical component of the HA-induced fusion mechanism.

Results

Influenza HA (strain A/PR/8/34) was reconstituted into supported lipid bilayers (viroplanes) on the surface of a germanium internal reflection plate as schematically depicted in Figure 1. We showed previously that reconstituted HA in this system is functional (Hinterdorfer *et al.*, 1994): the viroplanes specifically bind target membranes that bear sialic acid residues on their surfaces and they support fusion with appropriate target membranes.

Secondary structure of HA at pH 7.4

Polarized ATR-FTIR spectra of reconstituted HA in the presence and absence of target vesicles at pH 7.4 are shown in Figure 2. The most prominent bands, arising from protein or lipid, are assigned. The addition of target vesicles results in a substantial increase of the lipid

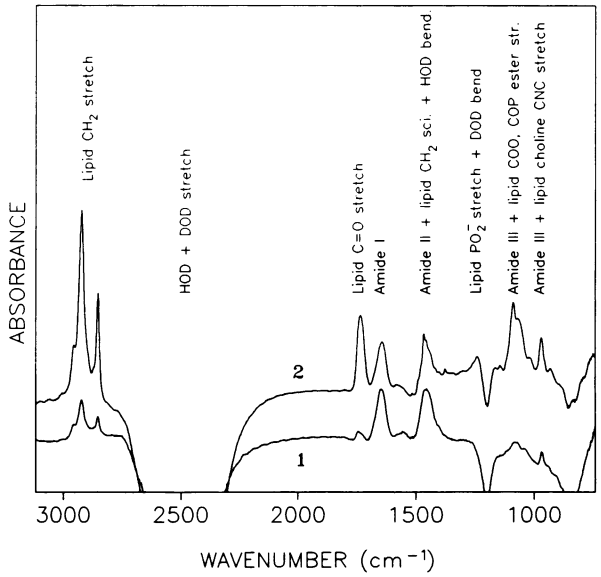

Fig. 2. ATR-FTIR spectra of reconstituted HA with and without bound target vesicles. Perpendicular polarized ATR-FTIR absorbance spectra of HA reconstituted in supported bilayers at pH 7.4 are shown in the absence (spectrum 1) and presence (spectrum 2) of bound POPC/CL (4:1, mol/mol) vesicles. The most prominent absorbance bands originating from lipid or protein vibrations are designated.

absorbance bands, which indicates that the reconstituted HA binds these vesicles at pH 7.4, in good agreement with our previous total internal reflection fluorescence study (Hinterdorfer *et al.*, 1994). The amide I′ band is of particular interest because the relative contents of different secondary structures can be obtained from an analysis of this band. Substructures of the amide I′ bands are revealed by calculating the fourth derivatives in this spectral region,

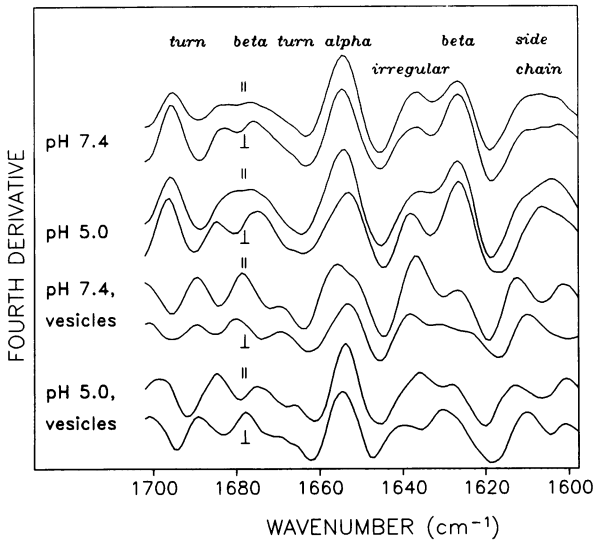

Fig. 3. Fourth derivative spectra of reconstituted HA in the amide I region under various experimental conditions. The spectra were recorded at parallel and perpendicular polarizations of the IR beam, at pH 7.4 and pH 5.0, and in the absence and presence of bound POPC/cardiolipin (4:1) vesicles, as indicated. The spectral regions corresponding to different secondary structures are assigned.

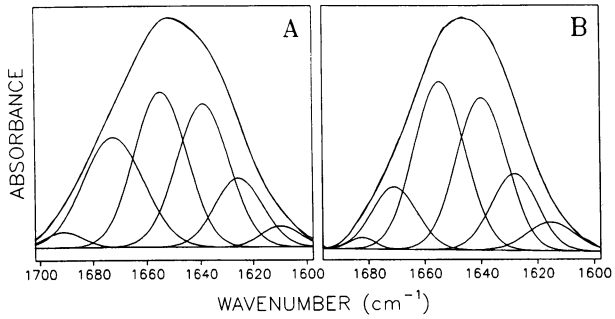

Fig. 4. Spectral decomposition of the amide I′ band of reconstituted HA in the absence and presence of target vesicles. Parallel polarized ATR-FTIR absorbance spectra of reconstituted HA are shown in the amide I region at pH 7.4 in the absence of target vesicles (**A**) and at pH 5.0 in the presence of bound POPC/CL (4:1) target vesicles (**B**). Six Gaussian component bands and their sums, resulting from curve-fitting (see text), are also shown in each case.

as shown in Figure 3. At least six peaks are found in all eight spectra of Figure 3. Several of these components can be assigned to specific secondary structures (Susi and Byler, 1986; Arrondo *et al.*, 1993; Surewicz *et al.*, 1993). The most pronounced peak occurs at ~1655 cm^{-1} and is assigned to α-helix. The components at ~1638 cm^{-1} and ~1625 cm^{-1} are attributed to irregular and β-structure, respectively. The position of the band assigned to α-helix indicates that the majority of the amide protons in helices are not deuterium-exchanged, because deuterated α-helices absorb at ~1645 cm^{-1} (Venyaminov and Kalnin, 1990; Zhang *et al.*, 1995). The peak at ~1610 cm^{-1} is most likely due to side chain vibrations. The assignment of the components between 1665 and 1700 cm^{-1} is less certain, because in this region several turn frequencies overlap with the high frequency counterpart of the split antiparallel β-sheet vibration (Krimm and Bandekar, 1986). To quantitate the relative amounts of secondary structure, the original amide I bands were curve-fitted with six Gaussian component bands using the positions of the fourth derivative peaks as input frequencies. The result of this fit for HA at pH 7.4 in the absence of target vesicles is shown in Figure 4A.

The sum of the Gaussian component bands is virtually indistinguishable from the experimental amide I′ band. The secondary structure of the reconstituted HA at pH 7.4, as calculated from the relative areas of the component bands, was ~30% α-helix, 12–29% β-sheet, 6–23% turns and ~35% irregular structure. These percentages are accurate to at least ±5%, as determined from the averages of four independent experiments. Because antiparallel β-sheets and turns contribute to the high frequency amide I′ region, we chose to represent this intensity with one broad, unresolved band at ~1672 cm^{-1} and, therefore, we report ranges for the percentages of β-sheet and turns. The lower limits of β-structure and turns were obtained from the component band areas at ~1625 and ~1690 cm^{-1}, respectively; the upper limits were obtained by adding the area of the band at ~1672 cm^{-1} to these fractions. Despite this uncertainty concerning the relative contributions of β-sheet and turns, all fractions of secondary structure determined by ATR-FTIR spectroscopy agree quite well with previous X-ray and CD results on strain X31 BHA, which has 22–23% α-helix, 28–34% β-sheet and 16% reverse turns (Wilson *et al.*, 1981; Wharton *et al.*, 1988b). When 24 α-helical residues are added for the transmembrane helix that is missing in BHA, one expects a helical content of ~26% for the whole HA molecule, which is in reasonable agreement with our FTIR results on the secondary structure of PR/8 HA.

Orientation of HA at pH 7.4

The orientation of HA relative to the plane of the membrane can be determined by measuring the ATR dichroic ratio (R^{ATR}) of the amide I′ band. R^{ATR} is the ratio of the height of the amide I′ band at parallel and perpendicular polarizations of the IR light. At pH 7.4 and in the absence of target vesicles, R^{ATR} was 1.90 ± 0.04 (average of 16 independent measurements). In order to determine the orientation of the HA molecules from this value, we calculated from Equation 2 (see Materials and methods for equations) the order parameter (S_H), which is a function of the orientational distribution of the α-helices of HA relative to the membrane normal (Equation 1). The two largest helices in the crystal structure of X31 BHA are oriented close to parallel to the trimer axis (Wilson *et al.*, 1981). From their C_α-coordinates, we calculated that these two helices, which comprise 53 and 19 residues, are oriented at 166 and 14° from the central axis of the HA trimer, respectively. The other helices are small and oriented at 47, 126, 84, 39 and 110° relative to the trimer axis and, therefore, do not contribute greatly to the total dichroic signal (see Discussion). We also expect ~24 residues of the transmembrane helix to contribute to the observed dichroism. Therefore, to a good approximation, 53 + 19 + 24 (= 96) of the total 550 residues will be in helices that are oriented approximately parallel (or antiparallel) to the trimer axis. With f_H = 96/550 = 0.175, we calculate S_H = 0.95 ± 0.19 for HA at pH 7.4 in the absence of target vesicles. The order parameter, as defined in Equation 1, can vary between the extreme values of +1 and –0.5, which correspond to orientations of the

Table I. Secondary structure of HA in the absence and presence of target vesicles determined by ATR-FTIR spectroscopy[a]

	No vesicles		POPC		POPC/POPG (3:2)		POPC/CL (4:1)	
	pH 7.4	pH 5.0	pH 7.4	pH 5.0	pH 7.4	pH 5.0	pH 7.4	pH 5.0
α-Helix[b]	30	29	30	39	28	39	30	40
β-Sheet[c]	12	16	15	13	16	15	18	24
β-Sheet[d]	0–17	0–15	0–14	0–13	0–15	0–14	0–17	0–13
Irregular[e]	35	34	35	28	38	32	29	21
Turn[f]	6–23	6–21	6–20	7–20	3–18	0–14	7–23	2–15

[a]The percentages of the amide I′ area excluding the side-chain component at ~1610 cm^{-1} are reported. The errors, as judged from at least four independent measurements, are ±5% or less in each case.
[b]The peak frequencies assigned to protonated α-helices are 1653–1655 cm^{-1}.
[c]Low frequency β-sheet component centered at 1625–1628 cm^{-1}.
[d]High frequency β-sheet component centered at 1670–1678 cm^{-1}; the total fraction of β-structure is the sum of the low and high frequency fractions that are assigned to β-sheet.
[e]The band centered at 1638–1640 cm^{-1} is normally assigned to deuterated 'random coil'. For a protein with a defined structure, we prefer to use the term 'irregular' structure to indicate aperiodic secondary structures that are neither helices, nor sheets, nor turns.
[f]Turn frequencies are ~1667, ~1683 and ~1694 cm^{-1}.

helices perpendicular and parallel to the membrane plane, respectively. Therefore, we conclude that the major α-helices and the HA trimers are oriented close to perpendicular to the plane of the membrane under these conditions.

Conformational change at pH 5

Influenza HA undergoes a well known acid-induced conformational change which leads to the exposure of the hydrophobic fusion peptide and eventually to a dissociation of the globular head domains within the HA trimer (Skehel *et al.*, 1982; Doms *et al.*, 1985; Tsurudome *et al.*, 1992; Bullough *et al.*, 1994). When we changed the pH from 7.4 to 5, the most dramatic change observed in the ATR-FTIR spectra of reconstituted HA was a decrease of the dichroic ratio of the amide I′ band. The dichroic ratio became 1.68 ± 0.04 at pH 5 in the absence of target vesicles. The relative contents of each secondary structure component were not changed much upon acidification, as is evident from the similarity of the corresponding fourth derivative spectra (Figure 3) and the decomposed amide I bands (not shown). Numerical values for the relative contents of each secondary structure under various experimental conditions are listed in Table I. These results agree with earlier studies using CD spectroscopy, which showed that the relative contents of secondary structures of BHA were similar at neutral and acidic pH (Skehel *et al.*, 1982; Wharton *et al.*, 1988b). The results are also consistent with the crystal structure of TBHA2 at pH 5, indicating that the total numbers of helical residues were similar in this fragment and in the corresponding portion of HA2 at pH 7, even though a major rearrangement of the α-helices occurred as a result of the conformational change (Bullough *et al.*, 1994). The TBHA2 fragment contains two major helices, 66 and 17 residues long, which are oriented at 169 and 34°, respectively from the trimer axis. Hence, the parameter f_H may be evaluated (i) taking only the longest helix (f_H = 66/550 = 0.12), (ii) taking the sum of the longest helix and the transmembrane helix, assuming that the latter remains parallel to the trimer axis [f_H = (66 + 24)/550 = 0.164], (iii) taking the sum of 66 and 17 residue helices [f_H = (66 + 17)/550 = 0.15], or (iv) taking all three helices [f_H = (66 + 17 + 24)/550 = 0.195]. Using these values of f_H, together with R^{ATR} = 1.68 ± 0.04, Equation 2 yields helical order parameters of S_H = –0.31 ± 0.33, –0.22 ± 0.24, –0.24 ± 0.27 and –0.18 ± 0.21, respectively. The mean values of these order parameters cover a distribution of angles between the helical axes and the membrane normal, ranging from 63 to 69°. If the statistical errors are included, this range broadens to 54–90°. Since the 53 residue helix of HA2 at neutral pH and the 66 residue helix at acidic pH have similar orientations with respect to the trimer axis (166 and 169°, respectively), the observed acid-induced inclination of the long α-helix directly indicates a profound pH-dependent orientational change of the HA trimers. This result is not very model-dependent, because models (i)–(iv) are all dominated by the long triple-stranded helical coiled-coil of TBHA2 and, therefore, yield similar tilt angles.

Binding of target lipid vesicles at pH 7.4 and lipid order

Target lipid vesicles bind to the supported viroplanes after injection into the sample cell, as indicated by a marked increase of the integrated absorbance of the lipid methylene stretch vibrations at 2800–3000 cm^{-1} (Figures 2 and 5A). When unilamellar vesicles composed of 1-palmitoyl-2-oleoyl-phosphatidylcholine (POPC) and cardiolipin [CL (4:1)] were injected at pH 7.4, the intensity of the integrated lipid bands increased ~6-fold. Smaller increases of ~5- and 3-fold were observed after injection of vesicles composed of POPC and 1-palmitoyl-2-oleoyl-phosphatidylglycerol [POPG (3:2)] or pure POPC vesicles, respectively. These vesicles remained bound to the viroplane after flushing the cell with 12 volumes of pH 7.4 buffer. As previously shown by total internal reflection fluorescence microscopy (Hinterdorfer *et al.*, 1994), the vesicles bound essentially irreversibly to the HA viroplanes.

Information on the orientational distribution of the lipids can be obtained from measurements of the order parameter of the lipid hydrocarbon chains (S_L) (Brauner *et al.*, 1987; Frey and Tamm, 1991; Hübner and Mantsch, 1991). Before vesicle binding, S_L representing the lipids in the supported membranes was 0.3 ± 0.1, which is a typical value for bilayers in the liquid-crystalline phase (Frey and Tamm, 1991; Tamm and Tatulian, 1993; Tatulian *et al.*, 1995).

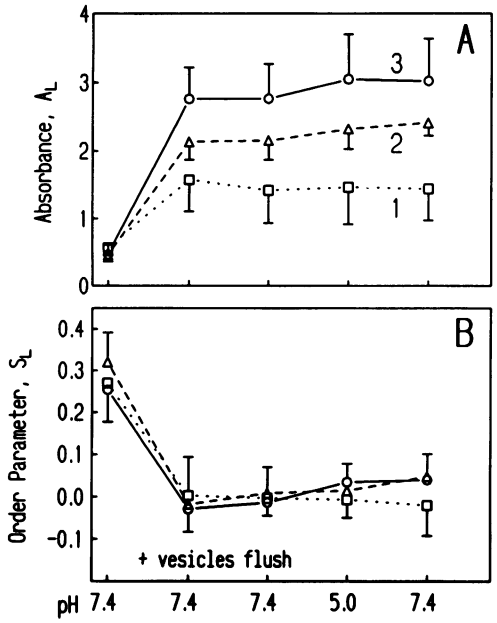

Fig. 5. Binding of target lipid vesicles to reconstituted HA in supported bilayers. Absorbance values, integrated from 2990 to 2810 cm^{-1}, which are due to lipid hydrocarbon chain CH_2 stretching vibrations (**A**), and the order parameter of the lipid hydrocarbon chains (**B**) are plotted as a function of the experimental conditions in a measuring sequence that consisted of the addition of target vesicles at pH 7.4, followed by three consecutive buffer exchanges using the pH 7.4, pH 5 and pH 7.4 buffers. The curves 1, 2 and 3 correspond to injected vesicles composed of POPC, POPC/POPG (3:2) and POPC/CL (4:1), respectively. The error bars designate the standard deviations calculated from three or four independent experiments.

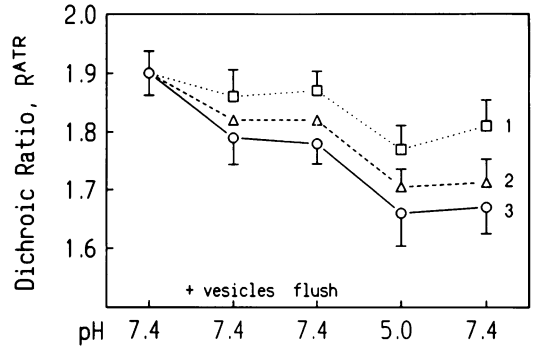

Fig. 6. ATR dichroic ratios of the amide I′ bands of reconstituted HA under different experimental conditions. The R^{ATR} values are plotted as a function of the experimental conditions in a measuring sequence that consisted of the addition of target vesicles at pH 7.4, followed by three consecutive buffer exchanges using the pH 7.4, pH 5 and pH 7.4 buffers. The curves 1, 2 and 3 correspond to injected vesicles composed of POPC, POPC/POPG (3:2) and POPC/CL (4:1), respectively. The error bars designate the standard deviations calculated from three or four independent experiments.

Binding of target lipid vesicles decreased the overall lipid order parameter to nearly zero, irrespective of the lipid composition of the vesicles (Figure 5B). When the cell was flushed after the vesicles had been bound with either pH 7.4 or pH 5 buffer, S_L was not noticeably changed. Since the lipid absorbance bands are dominated by the bound vesicles (Figure 5A), the low order parameter is primarily ascribed to these vesicles. An isotropic orientational distribution of lipids in spherical vesicles should indeed yield $S_L = 0$ (Equation 1). However, these results do not rule out changes in the organization of the lipids at the fusion junctions, because the contribution of these lipids to the total FTIR signal is negligible.

Conformation and orientation of HA in the presence of bound target membranes at pH 7.4

The relative contents of the spectrally resolved secondary structures of reconstituted HA did not change significantly after the binding of vesicles at pH 7.4 (Table I). Even though no major quantitative change in the secondary structure of HA appears to have occurred upon vesicle binding, smaller structural changes may still have been induced by the bound vesicles. This is evident, for example, from a comparison of the corresponding fourth derivative spectra of Figure 3. The observed small differences, although reproducible, are difficult to interpret. It is possible that there are more components contributing to the amide I′ band than the six that we could resolve with a reasonable degree of confidence.

The dichroic ratios of the amide I′ bands decreased from 1.90 to 1.78–1.87, depending on which lipid was bound to the viroplanes (Figure 6). Although smaller than those measured in the absence of bound target vesicles, the helical order parameters, calculated with $f_H = 0.175$, were 0.34–0.81, indicating predominantly vertical orientations of the HA trimers with bound target membranes at neutral pH.

Conformational change at pH 5 in the presence of bound target membranes

When the pH was changed from 7.4 to 5 after vesicle binding, we observed a significant increase of the spectral component at ~1655 cm^{-1} that has been assigned to α-helix (Figure 4B). About 30% helix was found at neutral and ~40% helix at acidic pH in the presence of target lipid membranes. Approximately the same increase of α-helical secondary structure was observed for all three types of lipid vesicles that were used in this study (Table I).

As in the absence of target vesicles, we observed a large decrease of the amide I′ dichroic ratio upon acidification in the presence of bound target vesicles (Figure 6). The R^{ATR} values, averaged from three or four independent measurements, were 1.66 ± 0.06, 1.70 ± 0.03 and 1.77 ± 0.04 for the POPC/CL, POPC/POPG and POPC vesicles, respectively. Using the mean values of R^{ATR} and the values 0.12–0.195 for f_H, as described above, the following helical order parameters are calculated: –0.29 to –0.47 for POPC/CL vesicles, –0.06 to –0.10 for POPC/POPG vesicles and 0.26–0.42 for POPC vesicles, which correspond to tilt angles from the membrane normal of 68–82°, 57–59° and 38–45°, respectively. The dichroic ratios of several typical measuring sequences and averaged from several independent experiments are shown in Figure 6. The same trends were observed for all three types of vesicles, although the negatively charged vesicles induced larger effects than the neutral POPC vesicles. A small decrease of R^{ATR} was always observed after vesicle binding at pH 7.4. Flushing the cell with pH 7.4 buffer had no significant effect on R^{ATR}. However, flushing the cell with pH 5 buffer led to a pronounced decrease of R^{ATR}, which remained low even after bringing the pH back to 7.4. This last step demonstrates that the average tilt angles of the

α-helices in HA were changed irreversibly by acidification in the presence of bound target membranes.

Discussion

We have studied the conformation of influenza HA reconstituted in supported phospholipid bilayers *in situ* by polarized ATR-FTIR spectroscopy. Our results show that the total secondary structure of reconstituted PR/8 HA is similar at pH 7.4, pH 5, and when complexed with target vesicles at pH 7.4 (Table I). Despite the ambiguities of the total percentages of β-structure and turns (which arise from unresolved amide I′ component bands in the 1665–1700 cm^{-1} spectral region), the agreement with the total secondary structures calculated from the crystal structure of X31 BHA (Wilson *et al.*, 1981) and determined by CD spectroscopy (Wharton *et al.*, 1988b) is quite good. The pH change in the absence of target vesicles and the binding of target vesicles at pH 7.4 apparently do not change the overall secondary structure of PR/8 HA significantly. Similarly, the total α-helical content of X31 BHA is not changed significantly upon acidification, as determined by CD spectroscopy (Skehel *et al.*, 1982; Wharton *et al.*, 1988b). When the pH was changed to 5 in the presence of bound target membranes, the total content of α-helical secondary structure increased from ~30% to ~40%. This corresponds to a transition of 50–60 residues to α-helices in the membrane-bound form of HA at pH 5. Part of this change is probably caused by some residues of the fusion peptide, which is non-helical in the pH 7 crystal structure (Wilson *et al.*, 1981), but forms an α-helix when bound to lipid vesicles (Lear and DeGrado, 1987; Wharton *et al.*, 1988a; Rafalski *et al.*, 1991). This still leaves ~40 residues of HA which become α-helical upon the acid-induced conformational change. This induction of additional helices in membrane-bound HA at the pH of membrane fusion has not been observed before, because in previous experiments the secondary structure of HA that was bound simultaneously to viral and target lipid bilayers has not been determined.

The most striking result of this study is the large increase of the tilt angle of the HA trimers as they undergo the conformational change at pH 5 in the presence or absence of target membranes. The orientation of reconstituted HA trimers at neutral pH and in the absence of bound vesicles is essentially perpendicular to the membrane plane, which is in agreement with the orientation of the HA spikes as observed in negatively stained or frozen hydrated electron micrographs (Ruigrok *et al.*, 1986; Booy, 1993). A decrease of the pH to 5 results in a tilt of the HA trimers toward the membrane surface by 60–70°. When the conformational change is induced in the presence of bound target vesicles containing 40 mol% POPG, a tilt angle similar to that in the absence of target membranes is observed (50–70°). The tilt angle appears to be larger in the presence of target vesicles containing 20 mol% cardiolipin (60–90°), and smaller when bound to pure POPC vesicles (30–50°). The large tilt obtained with CL-containing vesicles may be related to earlier observations that fusion of influenza viruses with such vesicles is very rapid and extensive, displays an unusual pH sensitivity, and therefore is probably not physiological (Stegmann *et al.*, 1989). Our result, that the tilt in the absence of target vesicles is larger than in the presence of POPC vesicles, implies that phosphatidylcholine (PC) target membranes partially interfere with the tilting motion of HA. This is consistent with earlier observations of poor fusion of influenza virus with pure PC bilayers (Stegmann *et al.*, 1985). Therefore, our results obtained with vesicles containing 40% POPG and yielding a tilt angle of ~60° should most closely represent the physiological situation. Unfortunately, the conformation and tilt angle of HA that is bound to vesicles which contain gangliosides, i.e. the physiological receptors for HA, cannot be measured with the current technique because gangliosides contain several amide groups which also absorb in the amide I region. However, we showed previously that POPC/POPG vesicles bound to and fused with supported planar HA-containing membranes as did vesicles composed of PC, phosphatidylethanolamine and the gangliosides G_{M1} or G_{D1a} (Hinterdorfer *et al.*, 1994).

The orientational order parameters that are determined from the IR dichroic ratios depend, to some extent, on the structural models that are used for their calculation, i.e. the fraction of α-helices that contribute to the measured dichroism. However, the model-dependent variations are small compared with the measured tilt angles. The contributions of the minor helices of the BHA structure are ~1%, as can be verified easily from their size and orientation within the crystal structure. For an error estimate of the orientation of the HA at pH 5 in the presence of target vesicles, we have to include the additional 50–60 residues that become α-helical under these conditions. We consider two extreme cases. First, if all 60 residues were in helices that are parallel to the trimer axis, the largest possible value of f_H is 0.195 + 60/550 = 0.30. In this case, the average helical tilt angles of HA bound to POPC/CL or POPC/POPG vesicles decrease by only 1–5° from 68 to 63° or from 58 to 57°, respectively. Second, if all 60 residues were in helices perpendicular to the trimer axis, the effective f_H decreases to 0.12–60/550/2 = 0.065. More negative S_H values are obtained, which result in tilt angles for the HA trimers of up to 90°. Therefore, we conclude that, irrespective of the orientation of the unknown helices of HA at pH 5, the observed acid-induced changes in the ATR dichroic ratio of the amide I′ bands yield tilt angles of at least 57–63° for the HA trimers at the pH of membrane fusion.

It should be noted that our measurements are not time resolved and therefore represent long-lived intermediates. It may well be that, due to steric constraints, fusion cannot go to completion in the supported bilayer system. Therefore, it is possible that a fusion intermediate which may appear only transiently in free membrane fusion has been stabilized in our system. It is also important to note that the reported order parameters are functions of the orientational distribution of all molecules in the system. Their interpretation with a single angle is just the most simple and most easily visualized representation. It is possible that two or more populations exist that give rise to the observed order parameters (averaged according to Equation 1). If there were mixed populations of HA in our system, some trimers would have to be tilted at even larger angles than the average angles reported here.

Our results have several implications for the architecture of the influenza HA fusion sites. Many models have been

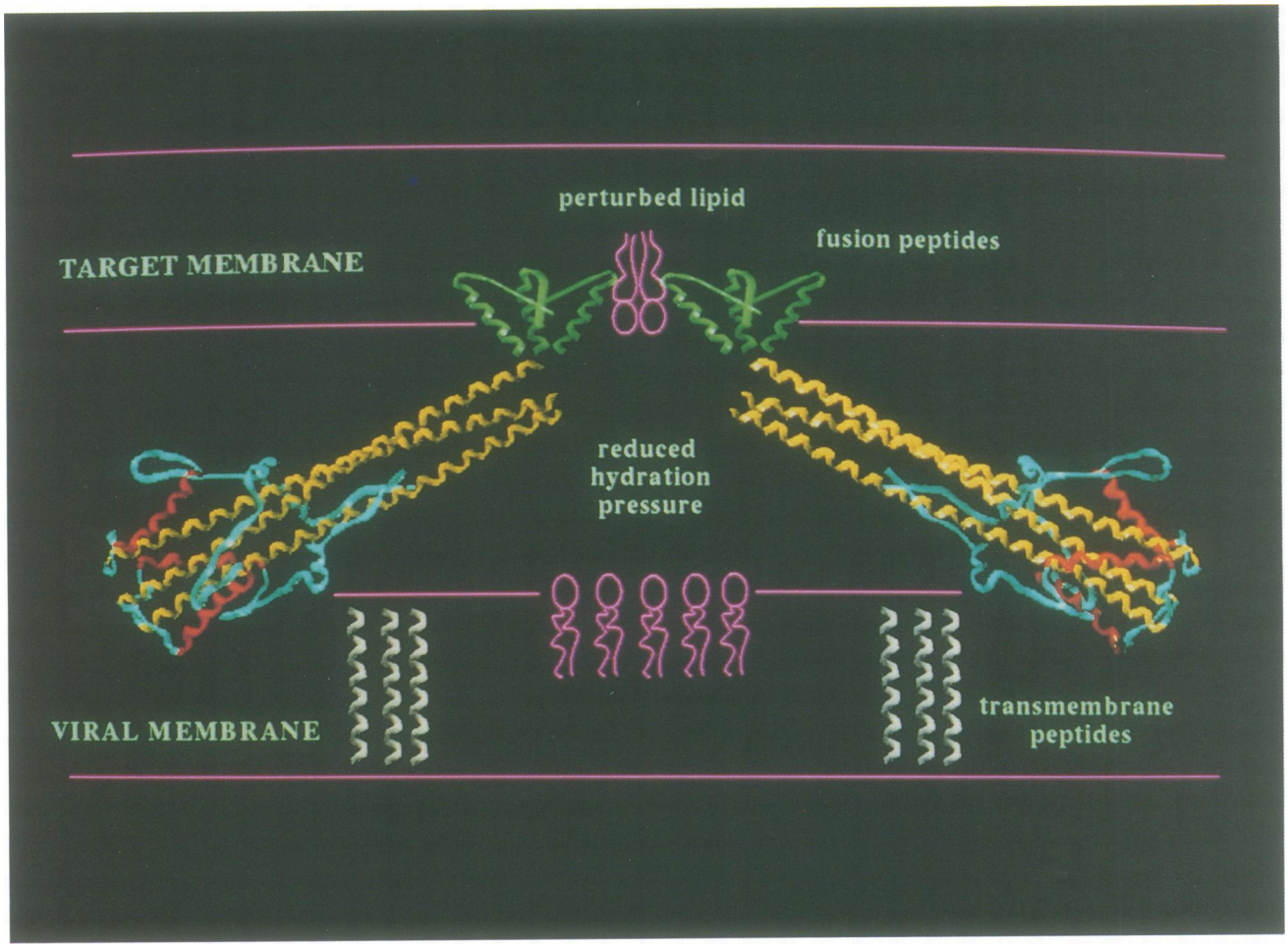

Fig. 7. Model of the pre-pore fusion intermediate formed by influenza HA in between two closely apposed membranes at pH 5. Several HA molecules assemble at the fusion site where, upon a decrease of the pH, they insert their fusion peptides into the target membrane and assume a tilted conformation (55–70° or more from the membrane normal). The net result is a closer appositon of the viral and target membranes. The fusion peptides perturb the lipid order in the target membrane, alter the water structure at the surface of the target membrane and reduce the hydration pressure in the fusion region. A detailed structure of the fusion peptides in the target membrane is not known, although there is evidence for α-helical and β-strand components. A fusion pore will form when the hydration pressure decreases below a critical threshold. The depicted model is based on the structure of TBHA2 (Bullough *et al.*, 1994). The HA1 chains (not shown) may be accommodated in the gap between the two membranes, but outside of the central fusion region. The lateral and angular positions of the transmembrane peptides in the viral membrane are not known. However, there is evidence that they also play an important role in the mechanism of HA-mediated membrane fusion (Kemble *et al.*, 1994). It is conceivable that, similarly to the fusion peptides, the transmembrane peptides perturb the viral lipid structure at the fusion site and thereby contribute to the reduction of the hydration pressure and the breakthrough of the fusion pore.

proposed for the HA fusion intermediate (Bentz *et al.*, 1990, 1993; Stegmann *et al.*, 1990; White, 1992; Siegel, 1993; Wilschut and Bron, 1993; Zimmerberg *et al.*, 1993; Stegmann, 1994). All of these relatively recent models incorporate experimental evidence that supports the recruitment of several HA trimers into each fusion site and the fact that the globular tops remain associated in the fusion intermediate. The models can be broadly classified into two categories, namely those that depict the HA trimers in an upright position, perpendicular to the planes of the two apposed membranes, and those that postulate a tilt of the HA trimers in the fusion sites. Most recently, a model was proposed in which the HA trimers were completely inverted, i.e. rotated through 180°, in the final fusion product (Wharton *et al.*, 1995). Our results clearly support the models with tilted HA trimers. The cited models further depict the fusion peptide exposed for interaction with lipids in the middle of the HA molecule, i.e. at approximately the same position where it is found in the pH 7 structure. Based on recent results by Carr and Kim (1993) and Bullough *et al.* (1994), it is more likely that, at pH 5, the fusion peptide is located at the end of the HA trimer that is most distal to its base and point of attachment to the viral membrane at pH 7. Bullough *et al.* (1994) further observed increased flexibility at the C-terminus of TBHA2, suggesting that at the pH of fusion the HA molecules might be able to bend with respect to the plane of the viral envelope, allowing a closer approach of the two membranes. The necessity of such an inclination, suggested also by Fuller (1994), is also consistent with the finding that the fusion peptides interact with the viral envelope upon acidification in the absence of target membranes (Weber *et al.*, 1994). In this work, we provide direct experimental evidence that reconstituted HA undergoes a profound inclination toward the viral membrane surface upon acidification in the presence or absence of bound target membranes. This bending motion is probably a critical step of HA-mediated membrane fusion and provides for a mechanism to bring the viral and target membranes into fusion contact.

In Figure 7 we present a model of a fusion intermediate that may be formed by HA in between the viral and target membranes at pH 5 before the two membranes merge and the fusion pore is opened. The model is based on the crystal structure of TBHA2 obtained at pH 5 (Bullough *et al.*, 1994) and incorporates our result of the tilted conformation at pH 5 when HA is bound to target membranes. The model also includes the observation (Brunner, 1989; Harter *et al.*, 1989; Stegmann *et al.*, 1991) that the fusion peptides insert into target membranes as amphipathic α-helices, although this contention has been challenged more recently (Gallaher *et al.*, 1992). The net effect of the tilt of the HA molecules is to bring the two membranes to be fused into closer apposition. The fusion peptides also alter the hydrogen bonding pattern of the lipid carbonyl groups in the fusion site (C.Gray, S.Tatulian, S.Wharton and L.Tamm, in preparation). We believe that these two changes, i.e. the close apposition of the two membranes and a possible alteration of the water structure in the gap between the membranes, could be two key elements of the mechanism of influenza HA-mediated membrane fusion.

Materials and methods

Materials

Influenza strain A/PR/8/34 was grown in the allantoic cavity of embryonated eggs and purified as described by Hinterdorfer *et al.* (1994). POPC and POPG (Na salt) were purchased from Avanti Polar Lipids (Alabaster, AL). CL extracted from *Escherichia coli* (Na salt, in $CHCl_3$) was from Sigma (St Louis, MO). D_2O was from Cambridge Isotope Laboratories (Woburn, MA). Bio-Beads SM2 from Bio-Rad Laboratories (Richmond, CA), and $C_{12}E_8$ from Calbiochem (San Diego, CA). All other chemicals were obtained from Sigma, Fisher (Fair Lawn, NJ), or Eastman Kodak (Rochester, NY).

Purification and reconstitution of HA in supported bilayers

Virus particles containing HA were prepared by solubilization of the viral envelope by $C_{12}E_8$, pelleting of the nucleocapsid by centrifugation and removing the detergent by Bio-Beads. Comparison of the SDS–PAGE patterns of the intact virus, the pellet and the purified HA proteoliposomes, performed under reducing conditions, showed that the nucleocapsid and the M protein were efficiently removed and the purified particles contained two components of apparent M_r 52 and 26 kDa, corresponding to HA1 and HA2 polypeptides, respectively (Hinterdorfer *et al.*, 1994). HA proteoliposomes were stored at −70°C in 5 mM HEPES, pH 7.4, containing 0.15 M NaCl.

Phospholipid bilayers supported on germanium internal reflection plates (50×20×1 mm^3 with 45° beveled edges, Buck Scientific, Norwalk, CT) were prepared as previously described (Frey and Tamm, 1991; Tamm and Tatulian, 1993). Briefly, a POPC monomolecular film was deposited onto the cleaned germanium plate from a Langmuir trough filled with pH 7.4 buffer at a constant surface pressure of 32 mN/m and the plate was assembled in a measuring cell. The HA proteoliposomes, diluted by pH 7.4 buffer to a protein concentration of ~30 μg/ml, were injected so that both surfaces of the monolayer-covered germanium plate were exposed to HA vesicles. The cell was incubated at room temperature for 2 h to allow the vesicles to fuse with the POPC monolayer and to yield a supported lipid bilayer with reconstituted HA. The excess unfused vesicles were flushed with 7 ml of D_2O buffer containing 5 mM HEPES, 10 mM MES, and 135 mM NaCl, pH 7.4. The pH of the buffers prepared in D_2O was adjusted without corrections for the isotope effect.

Preparation of vesicles

To prepare phospholipid vesicles of different composition, 850 nmol of total lipid [850 nmol of POPC, or 510 nmol POPC + 340 nmol POPG, or 680 nmol POPC + 170 nmol CL for pure POPC, POPC/POPG (3:2) and POPC/CL (4:1), respectively] dissolved in $CHCl_3$ were dried under a stream of N_2, 0.5 ml of pH 7.4 or pH 5.0 buffer (5 mM HEPES, 10 mM MES, and 135 mM NaCl in D_2O) was added, and the lipid was suspended by vortexing for 4–5 min. The lipid suspension was frozen and thawed five times using liquid N_2 and hot water, followed by 15 cycles of extrusion through a pair of 100 nm pore size polycarbonate membranes (Nucleopore, Pleasanton, CA) using a Liposofast extruder (Avestin, Ottawa, Canada).

Infrared spectroscopy

Polarized ATR-FTIR spectra were recorded on a Nicolet-740 FTIR spectrometer (Nicolet Analytical Instruments, Madison, WI) as previously described (Tamm and Tatulian, 1993; Tatulian *et al.*, 1995). Typically, 2000 scans were co-added at parallel and perpendicular polarizations of the IR beam at 2 cm^{-1} spectral resolution. Polarized ATR spectra of corresponding buffers, measured under similar conditions but in the absence of supported bilayers, were used as references. Before measurements, the instrument was purged with dry N_2 to remove H_2O vapor. The absorbance of residual H_2O vapor was subtracted to obtain a featureless baseline between 2100 and 1800 cm^{-1}, where neither protein nor lipid absorbs significantly. After recording the FTIR absorbance spectra of HA, the target phospholipid vesicles prepared in the respective buffers were injected to viroplanes to measure lipid binding and the effect of vesicle binding on the conformation of HA.

Processing of FTIR spectra

The ATR-FTIR spectra were processed using the Lab Calc software (Galactic Industries, Salem, NH). The baselines of amide I′ absorbance bands were corrected between 1700 and 1600 cm^{-1}. To identify the positions of the component peaks of the amide I′ band, the spectra were differentiated four times, accompanied by Savitsky–Golay smoothing. The peak wave numbers of the fourth derivative curves were used as starting parameters for curve fitting. For the identification of the frequencies of amide I component bands, any even-order derivative can be used; in most cases, the second derivatives have been used. In the case of HA, the second derivatives exhibited only a poorly expressed shoulder in the β-sheet region (~1635–1620 cm^{-1}). Therefore, we chose to employ the fourth derivatives, which reveal the major components of the secondary structure. The input full widths at half height of the individual Gaussian peaks were 12–22 cm^{-1}, depending on the width of the corresponding peak in the fourth derivative curve. Iterations were performed until good agreement between the simulated and experimental amide I′ bands ($\chi^2 < 10^{-6}$) was achieved. The results of amide I′ band decomposition were regarded as satisfactory if the difference between the starting and final wave numbers of the individual peaks did not exceed ~2 cm^{-1}. The relative contents of different secondary structure elements were estimated by dividing the areas of individual peaks, assigned to particular secondary structures, by the whole area of the resulting amide I′ band; the component around 1610 cm^{-1}, which is due to side chains, was not included in this procedure.

Order parameters

To describe the orientation of a structural element of a molecule in a uniaxial system such as a membrane, it is conventional to introduce an order parameter (S) which is a time- and space-averaged function of the angle θ between the principal axis of rotational symmetry of the structural element under consideration and the bilayer normal:

$$S = (3 \langle \cos^2\theta \rangle - 1)/2 \qquad (1)$$

The order parameter of an α-helix can be determined from the ATR dichroic ratio of the total amide I band, $R^{ATR} = A_\parallel/A_\perp$, where $A_\parallel$ and $A_\perp$ are the absorbances at parallel and perpendicular polarizations (Frey and Tamm, 1991).

$$S_H = \frac{1}{f_H S_\alpha} \frac{E_x^2 - R^{ATR}E_y^2 + E_z^2}{E_x^2 - R^{ATR}E_y^2 - 2E_z^2} \qquad (2)$$

In Equation 2, E_x, E_y and E_z are the Cartesian components of the electric field amplitude at the germanium–buffer interface, f_H is the fraction of α-helix in the molecule, $S_\alpha = (3\cos^2\alpha - 1)/2$, and α is the angle of the transition moment relative to the helix axis, i.e. 39° (Bradbury *et al.*, 1962; Tsuboi, 1962). For the conditions used in this and our previous work, and ignoring possible small changes due to dispersion in the spectral region of interest, $E_x^2 = 1.9691$, $E_y^2 = 2.2486$ and $E_z^2 = 1.8917$ (Tamm and Tatulian, 1993). The order parameter of the lipid hydrocarbon chains was calculated using (Frey and Tamm, 1991)

$$S_\perp = -2 \frac{E_x^2 - R^{ATR}E_y^2 + E_z^2}{E_x^2 - R^{ATR}E_y^2 - 2E_z^2} \qquad (3)$$

In Equation 3, R^{ATR} is the dichroic ratio of the symmetric (~2851 cm^{-1}) or antisymmetric (~2922 cm^{-1}) methylene stretching vibrations of the lipid hydrocarbon chains.

Acknowledgements

We thank Dr Judith White for critically reading the manuscript. This work was supported by grant R01 AI30557 from the National Institutes of Health. P.H. was a recipient of a Schroedinger postdoctoral fellowship from the Austrian government.

References

Arrondo,J.L.R., Muga,A., Castresana,J. and Goñi,F.M. (1993) Quantitative studies of the structure of proteins in solution by Fourier-transform infrared spectroscopy. *Prog. Biophys. Mol. Biol.*, **59**, 23–56.

Bentz,J., Ellens,H. and Alford,D. (1990) An architecture for the fusion site of influenza hemagglutinin. *FEBS Lett.*, **276**, 1–5.

Bentz,J., Ellens,H. and Alford,D. (1993) Architecture of the influenza hemagglutinin fusion site. In Bentz,J. (ed.), *Viral Fusion Mechanisms.* CRC Press, Boca Raton, FL, pp. 163–199.

Booy,F.P. (1993) Cryoelectron microscopy. In Bentz,J. (ed.), *Viral Fusion Mechanisms.* CRC Press, Boca Raton, FL, pp. 21–54.

Bradbury,E.M., Brown,L., Downie,A.R., Elliott,A., Fraser,R.D.B. and Hanby,W.E. (1962) The structure of the ω-form of poly-β-benzyl-L-aspartate. *J. Mol. Biol.*, **5**, 230–247.

Brauner,J.W., Mendelsohn,R. and Prendergast,F.G. (1987) Attenuated total reflection Fourier transform infrared studies of the interaction of melittin, two fragments of melittin, and δ-hemolysin with phosphatidylcholines. *Biochemistry,* **26**, 8151–8158.

Brunner,J. (1989) Testing topological models for the membrane penetration of the fusion peptide of influenza virus hemagglutinin. *FEBS Lett.*, **257**, 369–372.

Bullough,P.A., Hughson,F.M., Skehel,J.J. and Wiley,D.C. (1994) Structure of influenza hemagglutinin at the pH of membrane fusion. *Nature,* **371**, 37–43.

Carr,C.M. and Kim,P.S. (1993) A spring-loaded mechanism for the conformational change of influenza hemagglutinin. *Cell,* **73**, 823–832.

Clague,M.J., Schoch,C. and Blumenthal,R. (1993) Toward a dissection of the influenza hemagglutinin-mediated membrane fusion pathway. In Bentz,J. (ed.), *Viral Fusion Mechanisms.* CRC Press, Boca Raton, FL, pp. 113–132.

Doms,R.W., Helenius,A. and White,J. (1985) Membrane fusion activity of the influenza virus hemagglutinin. The low pH-induced conformational change. *J. Biol. Chem.*, **260**, 2973–2981.

Frey,S. and Tamm,L.K. (1991) Orientation of melittin in phospholipid bilayers. A polarized attenuated total reflection infrared study. *Biophys. J.*, **60**, 922–930.

Fuller,S. (1994) Influenza hemagglutinin: illuminating fusion. *Structure,* **2**, 903–906.

Gallaher,W.R., Segrest,J.P. and Hunter,E. (1992) Are fusion peptides really 'sided' insertional helices? *Cell,* **70**, 531–532.

Harter,C., James,P., Bächi,T. Semenza,G. and Brunner,J. (1989) Hydrophobic binding of the ectodomain of influenza hemagglutinin to membranes occurs through the 'fusion peptide'. *J. Biol. Chem.,* **264**, 6459–6464.

Hinterdorfer,P., Baber,G. and Tamm,L.K. (1994) Reconstitution of membrane fusion sites. A total internal reflection fluorescence microscopy study of influenza hemagglutinin-mediated membrane fusion. *J. Biol. Chem.*, **269**, 20360–20368.

Hübner,W. and Mantsch,H.H. (1991) Orientation of specifically $^{13}C{=}O$ labeled phosphatidylcholine multilayers from polarized attenuated total reflection FT-IR spectroscopy. *Biophys. J.,* **59**, 1261–1272.

Kemble,G.W., Danieli,T. and White,J.M. (1994) Lipid-anchored influenza hemagglutinin promotes hemifusion, not complete fusion. *Cell,* **76**, 383–391.

Krimm,S. and Bandekar,J. (1986) Vibrational spectroscopy and conformation of peptides, polypeptides, and proteins. *Adv. Prot. Chem.*, **38**, 181–364.

Lear,J.D. and DeGrado,W.F. (1987) Membrane binding and conformational properties of peptides representing the NH_2 terminus of influenza HA-2. *J. Biol. Chem.*, **262**, 6500–6505.

Rafalski,M., Ortiz,A., Rockwell,A., van Ginkel,L.C., Lear,J.D., DeGrado,W.F. and Wilschut,J. (1991) Membrane fusion activity of the influenza virus hemagglutinin: interaction of HA2 N-terminal peptides with phospholipid vesicles. *Biochemistry,* **30**, 10211–10220.

Ruigrok,R.W.H., Martin,S.R., Wharton,S.A., Skehel,J.J., Bayley,P.M. and Wiley,D.C. (1986) Conformational changes in the hemagglutinin of influenza virus which accompany heat-induced fusion of virus with liposomes. *Virology,* **155**, 484–497.

Siegel,D.P. (1993) Modeling protein-induced fusion mechanisms: insights from the relative stability of lipidic structures. In Bentz,J. (ed.), *Viral Fusion Mechanisms.* CRC Press, Boca Raton, FL, pp. 475–512.

Skehel,J.J., Bayley,P.M., Brown,E.B., Martin,S.R., Waterfield,M.D., White,J.M., Wilson,I.A. and Wiley,D.C. (1982) Changes in the conformation of influenza virus hemagglutinin at the pH optimum of virus-mediated membrane fusion. *Proc. Natl Acad. Sci. USA,* **79**, 968–972.

Stegmann,T. (1994) Anchors aweigh. *Curr. Biol.*, **4**, 551–554.

Stegmann,T. and Helenius,A. (1993) Influenza virus fusion: from models toward a mechanism. In Bentz,J. (ed.), *Viral Fusion Mechanisms.* CRC Press, Boca Raton, FL, pp. 89–111.

Stegmann,T., Hoekstra,D., Scherphof,G. and Wilschut,J. (1985) Kinetics of pH-dependent fusion between influenza virus and liposomes. *Biochemistry,* **24**, 3107–3113.

Stegmann,T., Nir,S. and Wilschut,J. (1989) Membrane fusion activity of influenza virus. Effects of gangliosides and negatively charged phospholipids in target liposomes. *Biochemistry,* **28**, 1698–1704.

Stegmann,T., White,J.M. and Helenius,A. (1990) Intermediates in influenza induced membrane fusion. *EMBO J.*, **9**, 4231–4241.

Stegmann,T., Delfino,J.M., Richards,F.M. and Helenius,A. (1991) The HA2 subunit of influenza hemagglutinin inserts into the target membrane prior to fusion. *J. Biol. Chem.*, **266**, 18404–18410.

Surewicz,W.K., Mantsch,H.H. and Chapman,D. (1993) Determination of protein secondary structure by Fourier transform infrared spectroscopy: a critical assessment. *Biochemistry,* **32**, 389–394.

Susi,H. and Byler,D.M. (1986) Resolution-enhanced Fourier transform infrared spectroscopy of enzymes. *Methods Enzymol.*, **130**, 290–311.

Tamm,L.K. and Tatulian,S.A. (1993) Orientation of functional and nonfunctional PTS permease signal sequences in lipid bilayers. A polarized attenuated total reflection infrared study. *Biochemistry,* **32**, 7720–7726.

Tatulian,S.A., Jones,L.R., Reddy,L.G., Stokes,D.L. and Tamm,L.K. (1995) Secondary structure and orientation of phospholamban reconstituted in supported bilayers from polarized attenuated total reflection FTIR spectroscopy. *Biochemistry,* **34**, 4448–4456.

Tsuboi,M. (1962) Infrared dichroism and molecular conformation of α-form poly-γ-benzyl-L-glutamate. *J. Polymer Sci.,* **59**, 139–153.

Tsurudome,M., Glück,R., Graf,R., Falchetto,R., Schaller,U. and Brunner,J. (1992) Lipid interactions of the hemagglutinin HA2 NH_2-terminal segment during influenza virus-induced membrane fusion. *J. Biol. Chem.*, **267**, 20225–20232.

Venyaminov,S.Y. and Kalnin,N.N. (1990) Quantitative IR spectrophotometry of peptide compounds in water (H_2O) solutions. II. Amide absorption bands of polypeptides and fibrous proteins in α-, β-, and random coil conformations. *Biopolymers,* **30**, 1259–1271.

Weber,T., Paesold,G., Galli,C., Mischler,R., Semenza,G. and Brunner,J. (1994) Evidence for H^+-induced insertion of influenza hemagglutinin HA2 N-terminal segment into viral membrane. *J. Biol. Chem.*, **269**, 18353–18358.

Wharton,S.A., Martin,S.R., Ruigrok,R.W.H., Skehel,J.J. and Wiley,D.C. (1988a) Membrane fusion by peptide analogues of influenza virus hemagglutinin. *J. Gen. Virol.*, **69**, 1847–1857.

Wharton,S.A., Ruigrok,R.W.H., Martin,S.R., Skehel,J.J., Bayley,P.M., Weis,W. and Wiley,D.C. (1988b) Conformational aspects of the acid-induced fusion mechanism of influenza virus hemagglutinin. Circular dichroism and fluorescence studies. *J. Biol. Chem.*, **263**, 4474–4480.

Wharton,S.A., Calder,L.J., Ruigrok,R.W.H., Skehel,J.J., Steinhauer,D.A. and Wiley,D.C. (1995) Electron microscopy of antibody complexes of influenza virus hemagglutinin in the fusion pH conformation. *EMBO J.*, **14**, 240–246.

White,J.M. (1992) Membrane fusion. *Science,* **258**, 917–924.

Wilschut,J. and Bron,R. (1993) The influenza virus hemagglutinin: membrane fusion activity in intact virions and reconstituted virosomes. In Bentz,J. (ed.), *Viral Fusion Mechanisms.* CRC Press, Boca Raton, FL, pp. 133–161.

Wilson,I.A., Skehel,J.J. and Wiley,D.C. (1981) Structure of the hemagglutinin membrane glycoprotein of influenza virus at 3 Å resolution. *Nature,* **289**, 366–373.

Zhang,Y.-P., Lewis,R.N.A.H., Henry,G.D., Sykes,B.D., Hodges,R.S. and McElhaney,R.N. (1995) Peptide models of helical hydrophobic transmembrane segments of membrane proteins. 1. Studies of the conformation, intrabilayer orientation, and amide hydrogen exchangeability of Ac-K_2-$(LA)_{12}$-K_2-amide. *Biochemistry,* **34**, 2348–2361.

Zimmerberg,J., Vogel,S.S. and Chernomordik,L.V. (1993) Mechanisms of membrane fusion. *Annu. Rev. Biophys. Biomol. Struct.*, **22**, 433–466.

Received on June 16, 1995; revised on July 24, 1995